Experimental investigation of flow over a backward facing step–progress report

By L. W. B. BROWNE[1]

Introduction

This report is a brief statement of the work contributed by the author to the backward-facing step experimental facility located in Test Cell No. 3 in the FML Building, N-260, at the NASA-Ames Research Center, during his sojourn with the Center of Turbulence Research — 3rd February to 28th August 1988. The work was carried out in close cooperation with Dr. Srba Jović, but since this is not a formal report of the Center of NASA-Ames, it has only a single author.

1. Wind Tunnel

Figure 1 shows the sizes and arrangement of the wind tunnel used for these experiments.

The sizes shown are for the final arrangement of the tunnel. They give an area contraction ratio of 9.4, a tunnel aspect ratio (width/height) of 2.17 and a step aspect ratio (tunnel width/step height) of 11.0.

In order to use temperature as a passive marker of the flow, it was considered desirable to have the floor of the tunnel heated to a uniform temperature of about 10°C above the free-stream temperature. This was accomplished by placing 6.3mm thick aluminium plates, with heaters, on the tunnel floor. These rest on spacers placed on the original plexi-glass floor and occupy the 1690mm and 2310mm lengths shown in Figure 1. The aluminium sheets have thin-foil heaters glued to their underside — the heaters being arranged to cover the whole surface of the aluminium. Four heating zones were provided, the voltage to each zone being controlled manually using a variac.

Approximately 40v A.C. has been found to give the required 10°C temperature difference when the free stream velocity is 10.0m/s. The plate temperatures are monitored using 13 thermocouples located on the center-line of the plate in small holes drilled to a depth of 5mm. A temperature distribution with a variation of less than $\pm$0.2°C over the whole plate can be achieved.

To provide a smooth entrance from the contraction section to the aluminium surface, the contraction section was raised until the aluminium surface and the contraction surface coincided. The resulting gap at the top of the tunnel was filled with a free-formed aluminium sheet held in place with duct tape.

1 Permanent Address: University of Newcastle

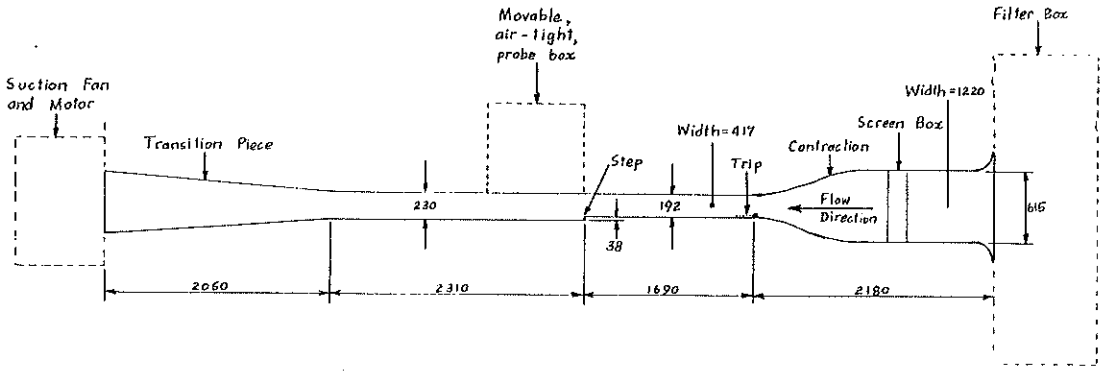

FIGURE 1. Layout and Sizes of Wind Tunnel

The flow was tripped, at the start of the aluminium plate, using a 1.6mm diameter rod followed by a 110mm width of 40 grit emery paper.

To provide an approximate zero pressure gradient flow, the sides of the tunnel were angled slightly outwards.

2. Air Flow

After the difficulties associated with trying to use the large (240,000 c.f.m.) FML compressor to provide a suction flow through a sonic nozzle, it was decided to install a standard suction fan system.

A general purpose fan, manufactured by the New York Blower Company, was purchased. This has a 460mm diameter fan wheel with airfoil-shaped blades capable of running at 2100 rpm. At a speed of about 800 rpm the required tunnel velocity of 10.0 m/s was achieved. As discussed later, this velocity provides an R_θ for the flow approaching the step of 1680. The fan is driven by an "Adjusto-Spede" eddy current clutch unit of the Eaton Corp. The motor (2 hp) runs at a constant 1130 rpm while a controlled current supply to the clutch provides variable speed at the output shaft. A model 3000 controller from the same company controlled the current.

Only 1/2 hp is required for the fan under our operating conditions, but the larger unit will allow other operating conditions to be considered. The single-turn potentiometer of the controller was replaced with a 10-turn unit with counter and was located adjacent to the experiment control area. This provides excellent speed control — the free stream velocity can be held steady, within $\pm 0.2\%$, over typically several hours of operation.

A transition piece between the end of the tunnel and the inlet to the fan was built (see Figure 1).

3. Cold-Wire Anemometers

Constant-current anemometers are commonly used with fine wires (typically 0.63μm diameter) to measure temperature fluctuations in turbulent flows. Ian

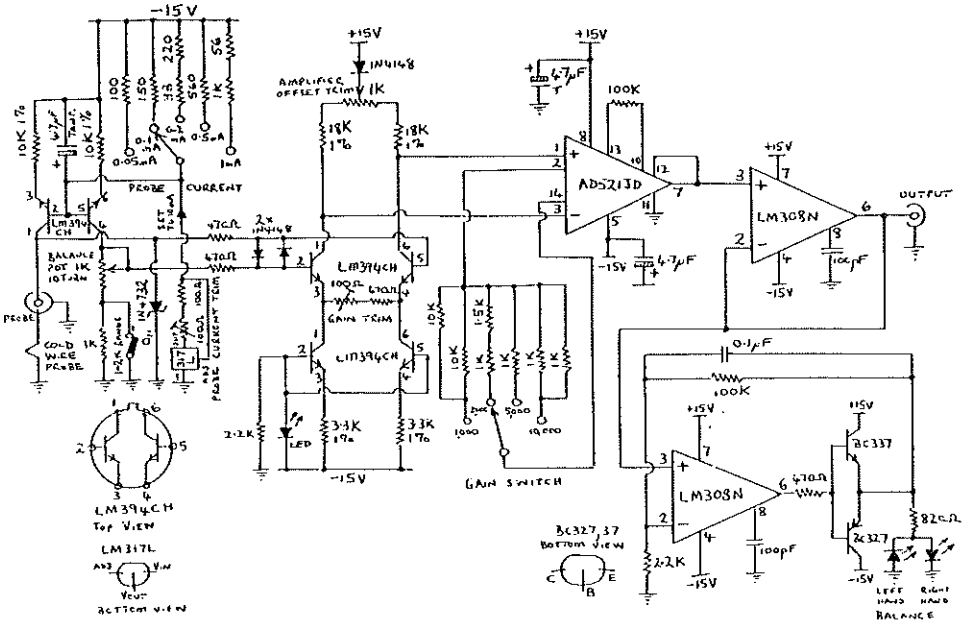

FIGURE 2. Circuit diagram of constant-current anemometer. (Designed by I. Miller — University of Newcastle, Australia)

Miller of the Dept. of Mechanical Engineering at the University of Newcastle has evolved, over the years, an excellent design for such units — See Figure 2.

Twelve circuit boards, one complete unit (to use as a guide), circuit diagrams, board layouts and instructions were supplied from Newcastle by Ian Miller and subsequently twelve constant-current anemometers were built at NASA-Ames. Some time was spent correcting problems (faulty components) but subsequent trials and use have shown the units to be operating very satisfactorily.

4. Hot-Wire Anemometers

Constant-temperature anemometers have also been developed by Ian Miller at the University of Newcastle — see Figure 3.

The signal to noise level of these units is as good as the best commercial units and their high frequency response ($\approx 25kHz$) is quite adequate, although not as high as can be achieved with the commercial units. Three complete units, five circuit boards, circuit diagrams, etc. were sent from Newcastle by Ian Miller. The three units are working very well, but due to parts supply problem, the other five units have not been completed. It may take another month to finish the five units. When these have been tested satisfactorily, the original three units will be returned to Newcastle.

5. Cold-Wire Rakes

Rakes of cold wires often provide the best means for the detection of coherent structures in a turbulent flow in which temperature has been added as a passive

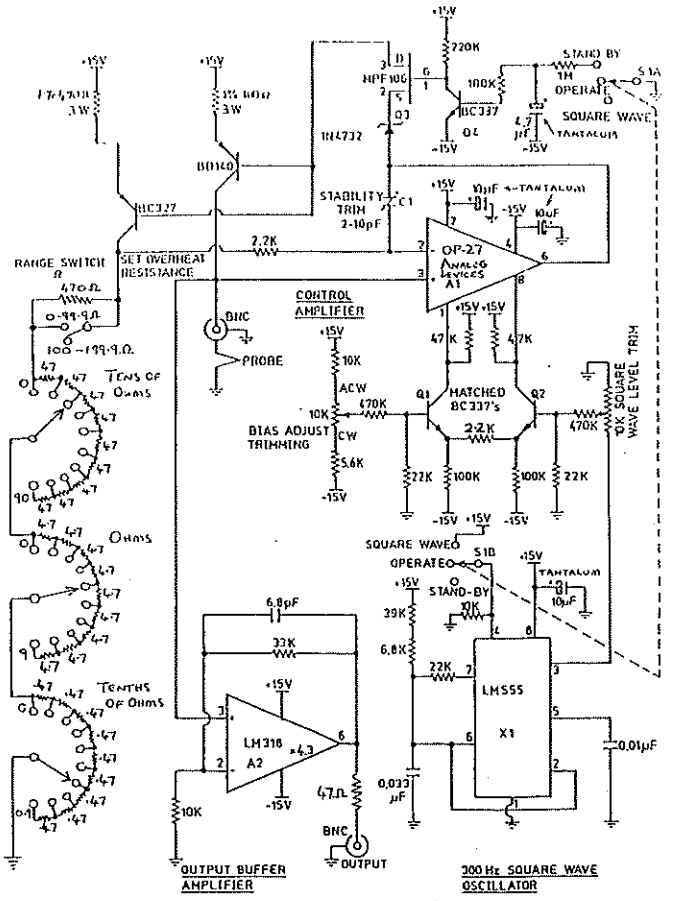

FIGURE 3. Circuit diagram of constant-temperature anemometer. (Designed by I. Miller — University of Newcastle, Australia)

scalar. Units, built at the University of Newcastle, and twelve plug-in probes were brought to NASA-Ames by the author. The units allow a 2-D array of wires to be used if required.

6. Wire Preparation

A facility for cold and hot wire preparation (soldering and etching) was developed.

7. Miniature 3-Wire Probe

To investigate near-wall structures, both in the upstream-of-step region and the downstream-of- reattachment region, it was felt that a miniature x-probe with an associated cold wire would be useful. Such a unit was built. The hot wires are 0.3mm long ($\approx 3L_k$ where L_k is the Kolmogorov length scale) separated by 0.2mm. The wires, 2.3μ m diameter platinum, are etched from

Wollaston wire and attached directly to the prongs. Their L/d of 130 is a little small, but from other work, were considered to be satisfactory.

To allow for more accurate measurements in the high turbulence intensity regions of the flow, the included angle between the wires was made 140° rather than the usual 90°. The cold wire is 0.63μm Pt - 10% Rh etched from a 1mm length of Wolluston wire soldered to prongs that can be moved forward and away from the x-wires to provide for easiest replacement of the wires. In its operating position, the cold wire is located in front and at right angles to the hot wires and as close as possible to them. The etched length of 0.5mm does not interfere with the flow over the hot wires.

8. Software

A number of programs were developed. These relate to instrument calibration, data taking, and data processing.

9. Results

9.1. Mean Free-Stream Velocities

Using a Pitot-tube it was found that the free-stream velocity, of 10m/s, outside the boundary layers on all surfaces of the tunnel, was uniform at any x position with $\pm$0.2%. There was a slightly favorable pressure gradient from the trip to the step, the center-line-mean velocity increasing by 0.3m/s over that distance (1690mm). A reference point for measuring the free stream velocity was established at 300mm upstream of the step.

9.2. Spanwise Velocity Variations in Boundary Layer Upstream of Step

The spanwise velocity variations in the floor boundary layer were typical of wind tunnel flows. Figure 4 shows the velocity variations, obtained with a Pitot tube, at $x = -225$mm (i.e. 225mm upstream from the step), at two distances from the wall.

The same patterns exist right through the boundary layer at any x position between the trip and the step (see Figure 5).

Note that the peaks and valleys of the variations occur consistently at the same z locations at all x positions and at any position in the boundary layer. It is also interesting to note that the same velocity variation patterns exist in the boundary layer before it arrives at the trip (see Figure 6).

Swearingen and Blackwelder (1987) found similar patterns of spanwise variations of the mean velocity in a wind tunnel boundary layer.

Bradshaw (1965) and Mehta and Hoffmann (1987) carried out investigations of this phenomena. The results they obtained changed whenever the last screen in the screen box was changed (or even when the last screen was vacuum cleaned), but the spanwise variations were always present. The best results obtained by

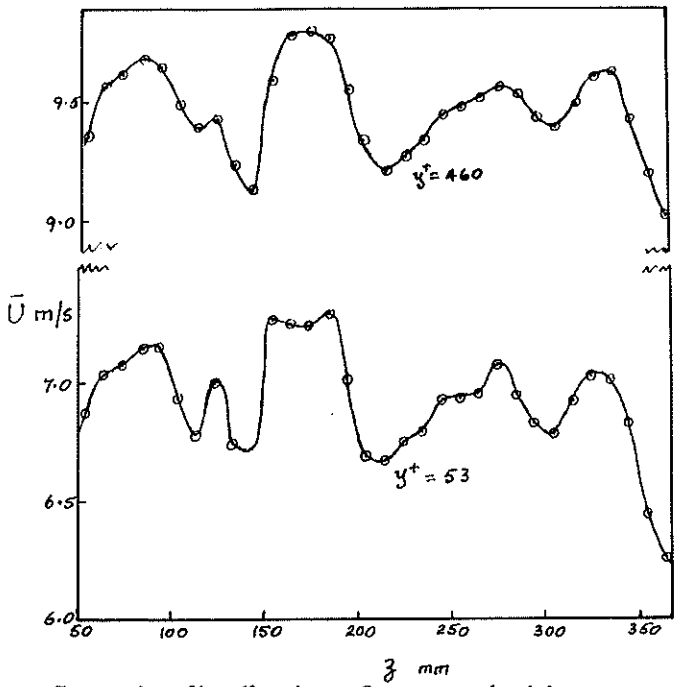

FIGURE 4. Spanwise distribution of mean velocities at $x = -225$mm at two positions in the boundary layer.

Mehta and Hoffmann (1987) was a $\pm 5\%$ peak to peak variation in the spanwise values of C_f, although a $\pm 17\%$ variation with earliest screens had been measured. We obtained a $\pm 7\%$ variation in the spanwise values of C_f at $x/H \approx -6$ (H is the step height), see Figure 7, and considered this to be satisfactory.

It was decided to carry out all future measurements at a z of 252mm. This point was still near the centre-line position ($z = 208$mm) and lay on the C_f curve at a point where the values were not changing too rapidly.

Note that (Mehta, verbal communication), since the spanwise variations are due to the final screen, (essentially there is some agglomeration of the streamwise vortices formed by the screen) a boundary layer developed on a plate placed centrally in the wind tunnel still has similar spanwise variations in the velocity and C_f values.

Recently, at a Berlin Conference (Second European Turbulence Conference, Aug. 30-Sept. 2, 1988, Techmische Universitat Berlin) Dengel and Fernholz (1988) reported that they had reduced C_f variations, caused by screens, from $\pm 15\%$ to 1% by using special "well behaved and carefully selected screens." Their final screen was produced by stamping rectangular holes in a piece of sheet metal — the sheet being about 0.5mm thick and the holes having a size of about 8mm × 5mm with their centre-lines being on a grid of about 11mm × 8mm. The solidity was thus about 0.4 - close to the norm for wind tunnel design.

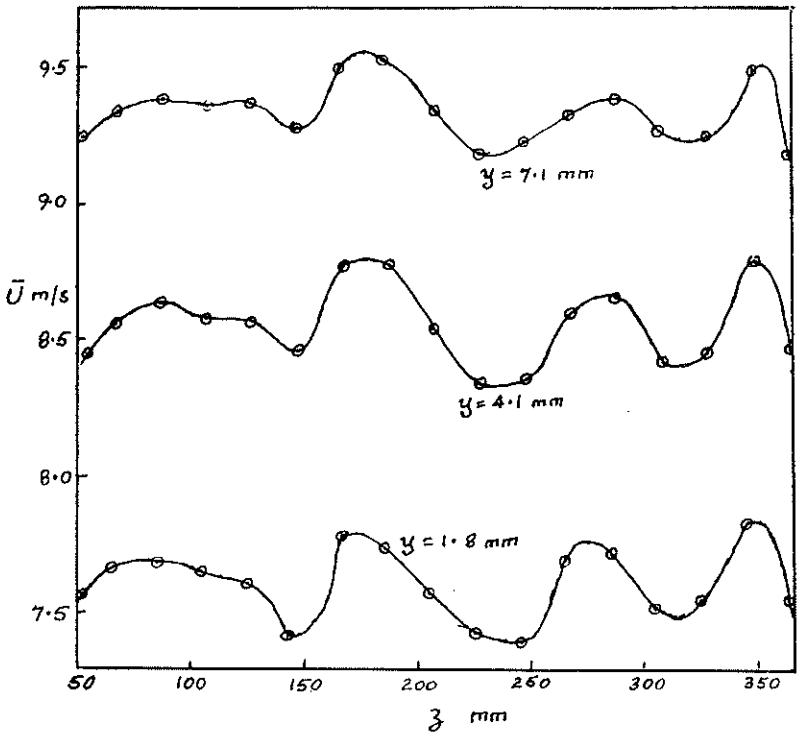

FIGURE 5. Spanwise distribution of mean velocities 355mm downstream of the trip at three positions in the boundary layer.

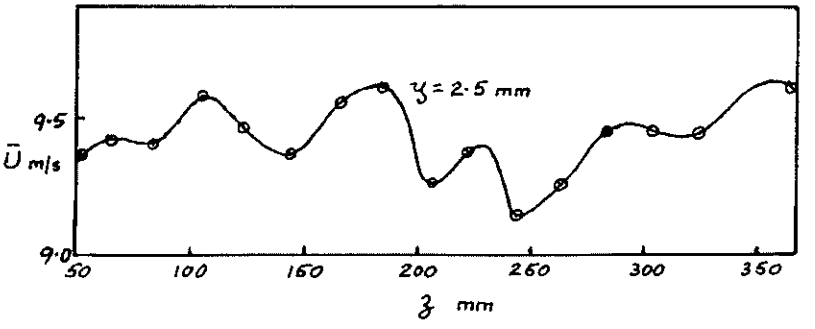

FIGURE 6. Spanwise distribution of mean velocities 10mm upstream of the trip at one position in the boundary layer.

9.3. Fully-Developed Nature of the Flow Upstream of the Step

In order to determine whether the flow had become "fully developed" as it approached the step, and also to check some of the instrumentation, it was decided to obtain profiles through the boundary layer at $x/H \approx -6$ (actual x position was -225mm) using a Pitot tube, a single hot wire, the miniature X-probe and a standard Disa X-probe (wire $d = 5\mu$m, $l = 1.25$mm). To ensure that there was no upstream influence of the step at this point, the step was later

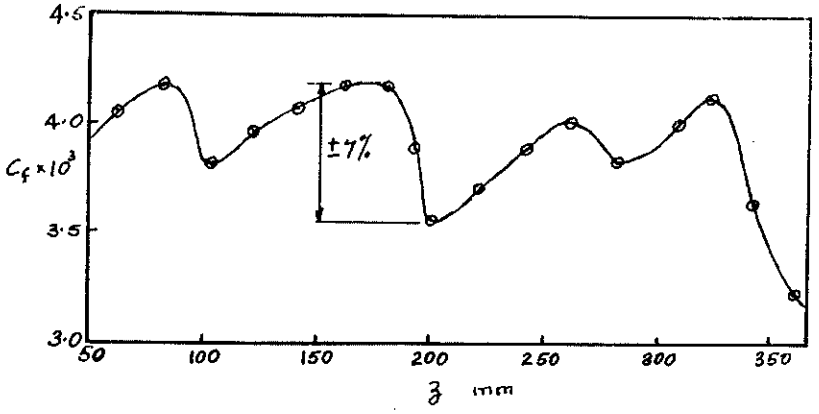

FIGURE 7. Spanwise distribution of C_f values at $x/H \approx -6$

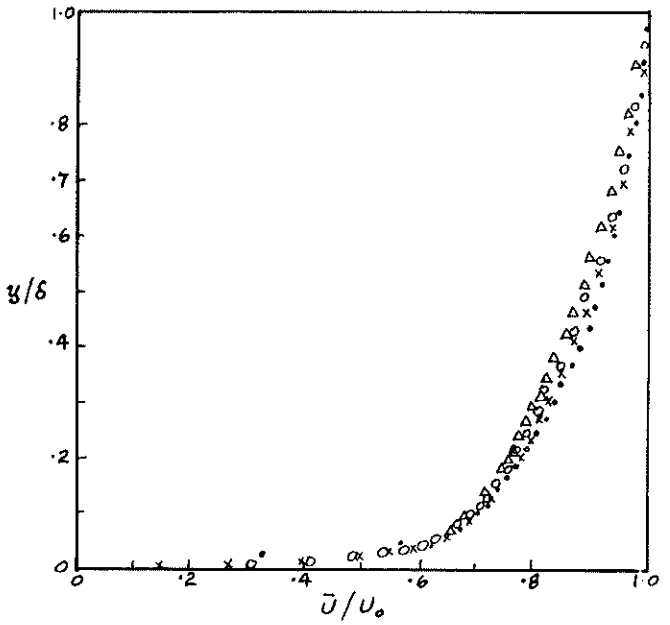

FIGURE 8. Mean velocity distribution across the boundary layer at $x/H \approx -6$. · Pitot; × Single hot wire; o Miniature X-probe; △ Disa X-probe.

"removed" by placing a length of ply-wood, in the downstream section of the tunnel, level with the upstream section, and the profile measurements were then repeated.

All mean velocity $\overline{U}$ profiles, plotted using outer layer values for non-dimensionalizing, gave good agreement — Figure 8.

To compare the velocity profiles using wall variables, it was necessary to determine the local C_f value. This was obtained by three different methods:

a) Using a Preston tube. The one we used was a flattened tube of height 0.252mm. (Subsequently, it was found that this corresponded to a height of $y^+ \approx 7$). The data was reduced using the Patel (1965) correlation equations.

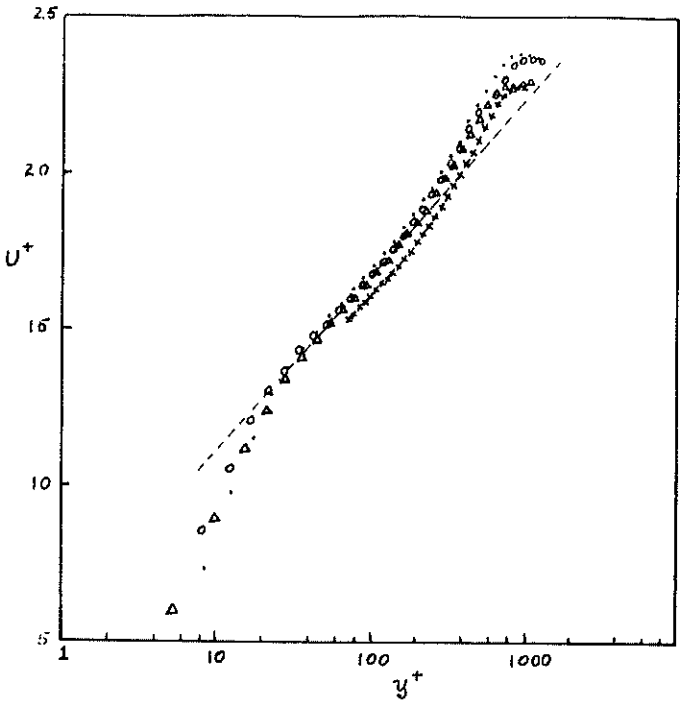

FIGURE 9. Mean velocity distribution across the boundary layer at $x/H \approx -6$. · Miniature X-probe with step; ○ Miniature X-probe without step; △ Single hot wire; × DIASA X-probe; — Best fit in log region.

b) Using the Clauser (1954) charts. These are based on

$$U^+ = \frac{1}{0.41} ln y^+ + 5.1$$

c) Using the Coles (1962) curves of R_θ vs C_f. From the mean velocity profiles, a momentum thickness, θ, of 2.55mm was obtained at $x/H \approx -6$ so that, for the flow at this position, $R_\theta = 1680$.

The results from the three methods were:

a) $C_f = 3.854 \times 10^{-3}$
b) $C_f = 3.925 \times 10^{-3}$
c) $C_f = 3.810 \times 10^{-3}$

A mean value of $C_f = 3.86 \times 10^{-3}$ was therefore used. This gave $u_\tau = 0.44$m/s for a free stream velocity of 10.0m/s. The resulting velocity profiles, normalized using wall values, are shown in Figure 9.

The curves are in good agreement except for the DISA probe. All curves have not been shown in Figures 8 and 9, but it was clear that the curves obtained with and without step were practically identical. The best fit straight line in the log region (Figure 9, neglecting the DISA results) is:

$$U^+ = \frac{1}{.404} ln y^+ + 5.35$$

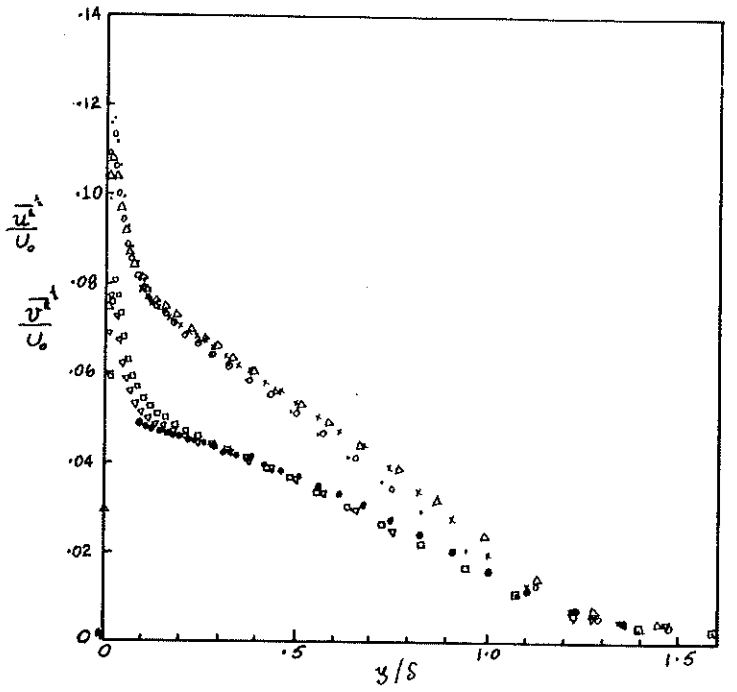

FIGURE 10. Distribution of $\overline{u^2}^{1/2}$ and $\overline{v^2}^{1/2}$ across the boundary layer at $x/H \approx -6$ (Outer scaling).
$\overline{u^2}^{1/2}$: · Miniature X-probe with step; ○ Miniature X-probe without step; △ Single hot wire; × DISA X-probe
$\overline{v^2}^{1/2}$: □ Miniature X-probe with step; ▽ Miniature X-probe without step; • DISA X-probe.

which is close to the fully developed case.

The strength of the wake, using the miniature X-probe results, is $\Delta U^+ = 1.4$. For a zero pressure gradient, Cole's (1962) curve of π vs R_θ gives a wake strength of 1.90 for $R_\theta = 1680$. Our wake strength indicates a slightly favorable pressure gradient.

Based on the mean velocity profiles, it would appear that at 6 step heights upstream of the step, the flow is close to the fully developed state and that there is no influence of the step on the flow.

9.4. Turbulence Quantities in Boundary Layer Upstream of Step

Turbulence quantities from the single hot wire, from the miniature X-probe and from the DISA X-probe, obtained at the six step heights upstream of the step position, were compared with one another with published data.

The $\overline{u^2}^{1/2}$ results are shown in Figure 10 using outer scaling and in Figure 11 using inner scaling.

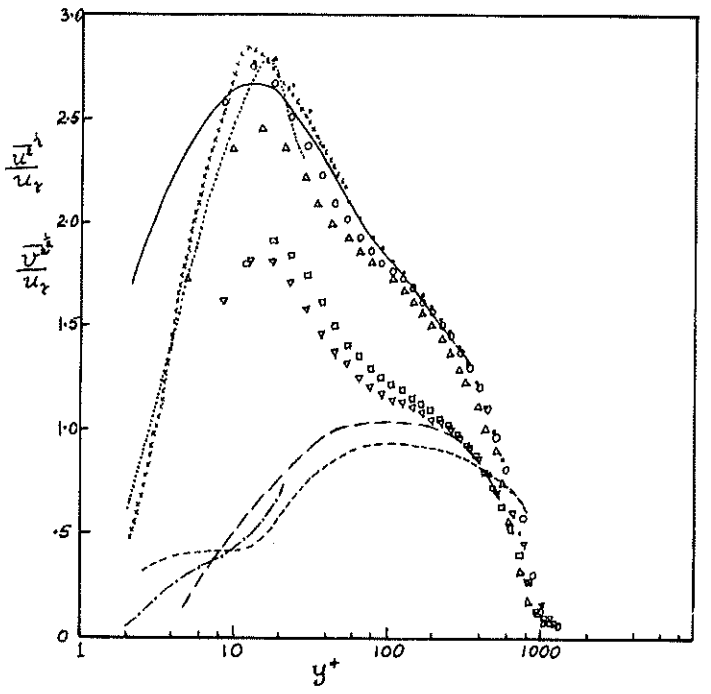

FIGURE 11. Distribution of $\overline{u^2}^{1/2}$ and $\overline{v^2}^{1/2}$ across the boundary layer at $x/H \approx -6$ (Inner scaling). Symbols as for Figure 10.
$\overline{u^2}^{1/2}$: — Spalart (1988); ··· Eckelmann (1974); × × × Andreopoulos et al. (1984).
$\overline{v^2}^{1/2}$: – – – Spalart (1988); –·–·– Eckelmann (1974); - - - - Andreopoulos et al. (1984)

All values in Figures 10 and 11 appear to be reasonable except for the $\overline{v^2}^{1/2}$ values obtained with the miniature X-probe. For this probe, the values obtained between $y^+ = 10$ to $Y^+ = 100$ ($y = .36$ to 3.6mm) are much higher than the usual values reported in the literature. Perry et al (1987) reported on and discussed at some length the difficulty of obtaining consistent v^2 measurements in the inner regions of boundary layers. Their survey of 13 published results for smooth-wall boundary layers shows the scatter of results obtained and is reproduced in Figure 12, together with the value that we obtained at that position in the boundary layer.

Our maximum value agrees with the values reported at higher von Kasman numbers. These discrepancies need further investigation for clarification, although it should be noted that the "non-isotropy," indicated by the difference between the $\overline{u^2}$ and $\overline{v^2}$ values, seems rather high for the curves drawn in Figure 11.

The $\overline{uv}$ results are shown in Figure 13 using outer scaling and in Figure 14

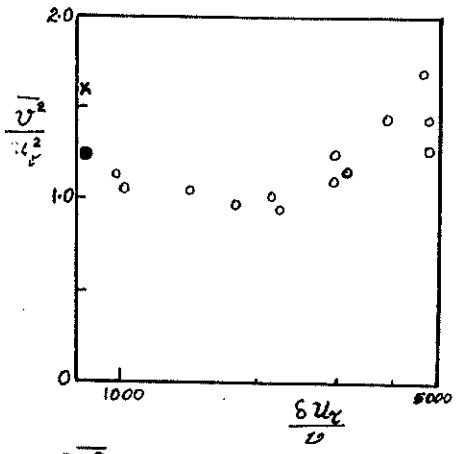

FIGURE 12. Values of $\overline{v^2}$ reported in the literature at $y/\delta = 0.1$ in a smooth-wall turbulent boundary layer. [Perry et al (1987)].
o Literature values — see Perry et al (1987) for details;
• Value obtained with miniature X-probe at $Y/\delta = .1$.
× Maximum value obtained with miniature X-probe.

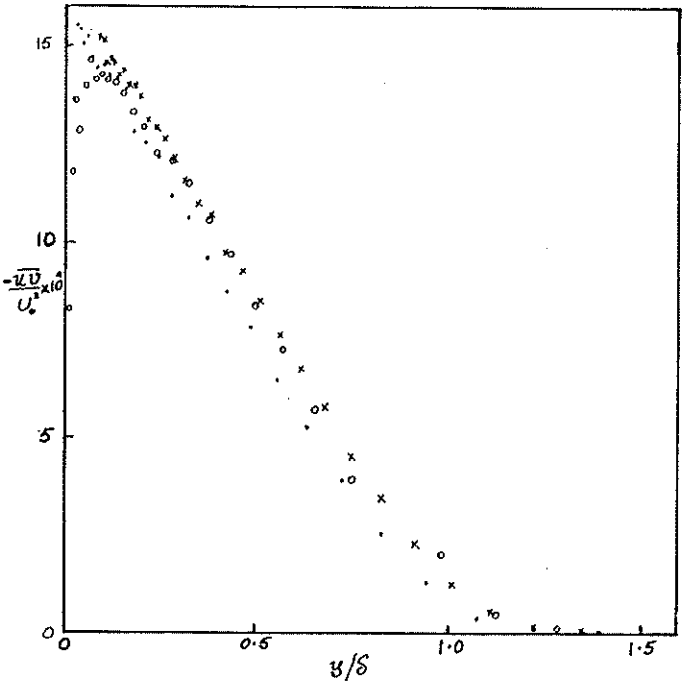

FIGURE 13. Distribution of $-\overline{uv}$ across the boundary layer at $x/H \approx -6$ (Outer scaling).
· Miniature X Probe with step; o Miniature X-probe without step; × DISA X-probe.

using inner scaling.

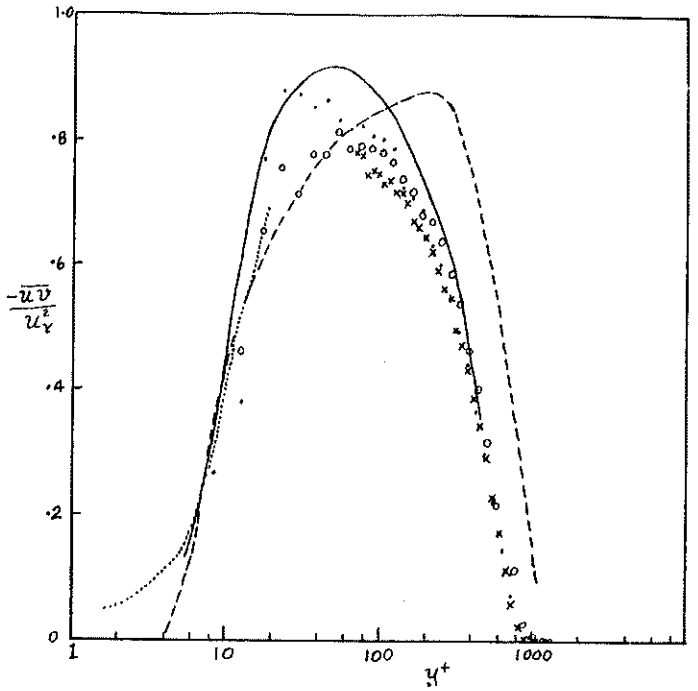

FIGURE 14. Distribution of $-\overline{uv}$ across the boundary layer at $x/H \approx -6$ (Inner scaling).
· Miniature X-probe with stop; o Miniature X-probe without step; × DISA X-probe.
— Spalart (1988); ··· Eckelmann (1974); - - - Andreopoulos et al (1984).

Except for the Andreopoulos et al (1984) curve in the outer regions of the flow, all results show reasonable agreement for the $\overline{uv}$ values. It is perhaps a little strange that results which are in agreement in $\overline{u^2}^{1/2}$ (Figure 11) and $\overline{uv}$ (Figure 14) should be so different in the $\overline{v^2}^{1/2}$ values (Figure 11).

9.5. Characteristics of Tunnel Flow Approaching Close to Step

When the Preston tube was traversed in the X direction along the plate (at $z = 252$mm — our standard z position) from $x = -350$mm to the lip of the step, we were surprised to find significant departures of C_f from the expected values — see Figure 15.

This seemed to indicate an upstream influence of the step and, from published work on backward facing step flows, such an influence had not been expected. Consequently, using the C_f curve as a guide, five stations ($x/h = -2.6, -1.5, -0.53, -0.13$, and $-0.$) were selected for detailed profile studies. Since the miniature X-probe had given reasonable results, it was used for these profiles in order to allow measurements to be made as close to the wall as possible.

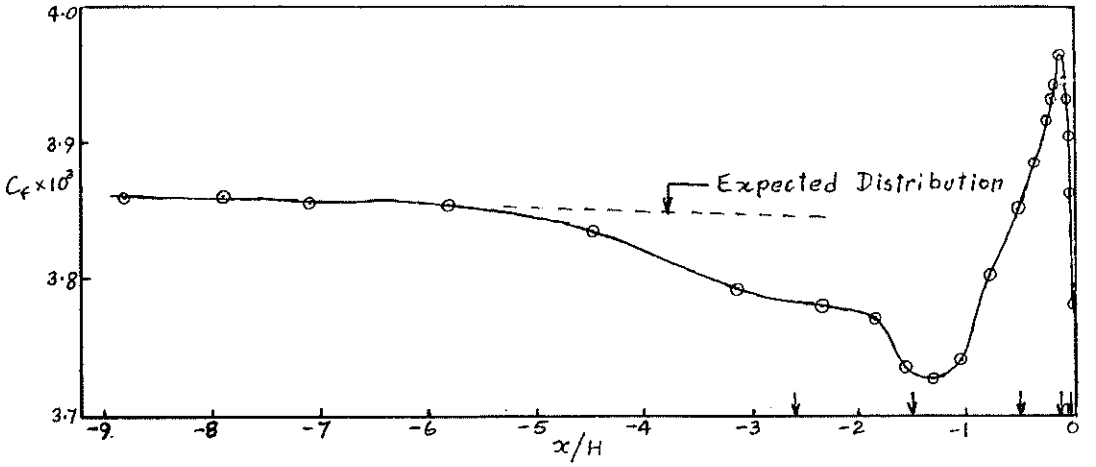

FIGURE 15. Distribution of C_f values near and upstream from the step. The arrows indicate stations where detailed profiles were taken.

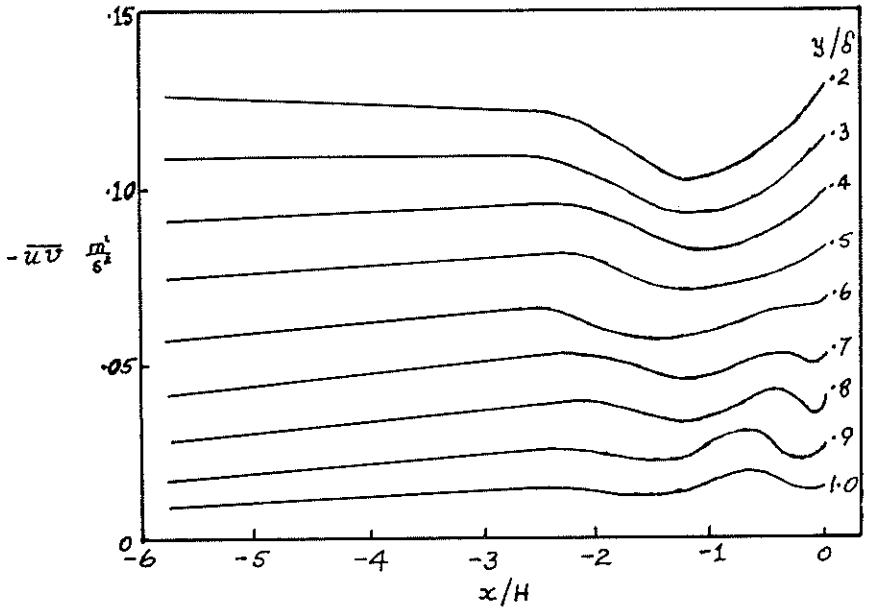

FIGURE 16. Distribution of $\overline{uv}$ in the outer regions of the boundary layer, upstream from the step.

The changes indicated by the C_f profile (Figure 15) were reflected in the turbulence quantities - in particular in the $\overline{uv}$ values, as shown in Figures 16 and 17.

The minimum of $-\overline{uv}$ in the inner part of the flow, Figure 17, occurs at approximately the same point ($x/H = -1.4$) as the minimum in the C_f curve, Figure 15. In the outer part of the flow, Figure 16, there are obviously some complex changes occurring in the large scale structures. The negative values of $-\overline{uv}$ that were measured at $y^+ = 10$ cannot be substantiated at this stage and

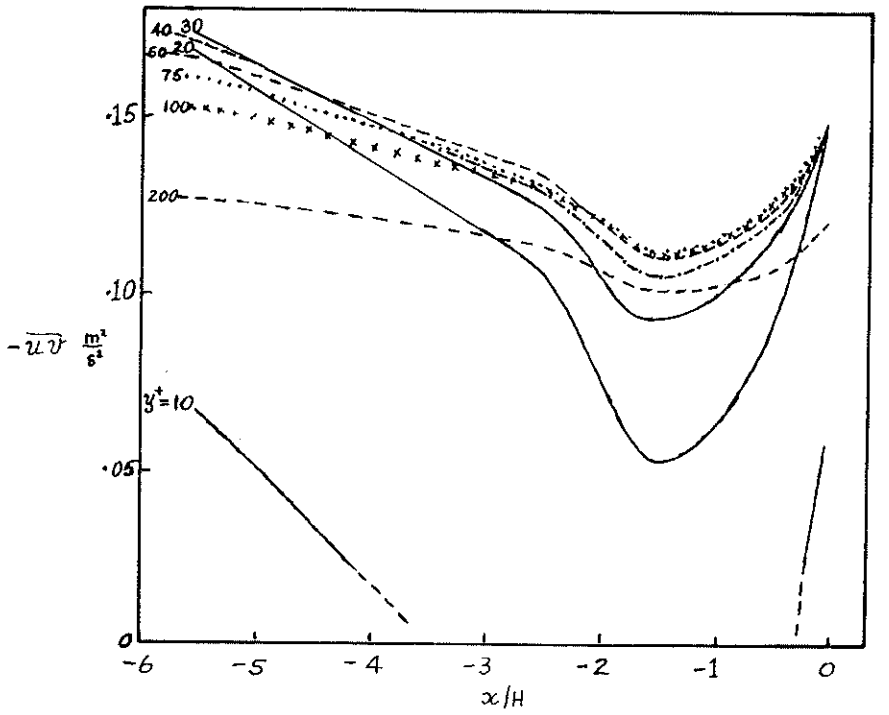

FIGURE 17. Distribution of $\overline{uv}$ in the inner regions of the boundary layer, upstream from the step.

may be due to the problems associated with X-wire measurements so close to the wall. A probe with wires of say 0.63μm diameter and 0.1mm long may be required to resolve this region.

The mean $\overline{v}$ velocities also follow the changes in the C_f curve, although in the opposite sense - peaking at minimum C_f and reaching a minimum at maximum C_f, Figure 18.

This upstream influence of the step does not seem to have been previously reported in the literature, although three instances of support for our results have been obtained:

a) In discussions with Dave Driver, he said that he had observed, in his work on the backward facing step, an increase in C_f (one data point) as the step was approached. This point was shown in the paper of Monson et al (1981) but was not commented on. The C_f values for their flow were different to ours, but by shifting the C_f origin and using the boundary layer thickness for non-dimensionalizing the distance from the step, some agreement is obtained between their C_f values and ours - see Figure 19.

   It is interesting to note that Monson et al (1981) obtained their C_f values using laser interferometry - a completely different technique to the Preston tube approach that we used.

b) In 1981, M. Sindir carried out, for NASA-Ames, numerical simulation work,

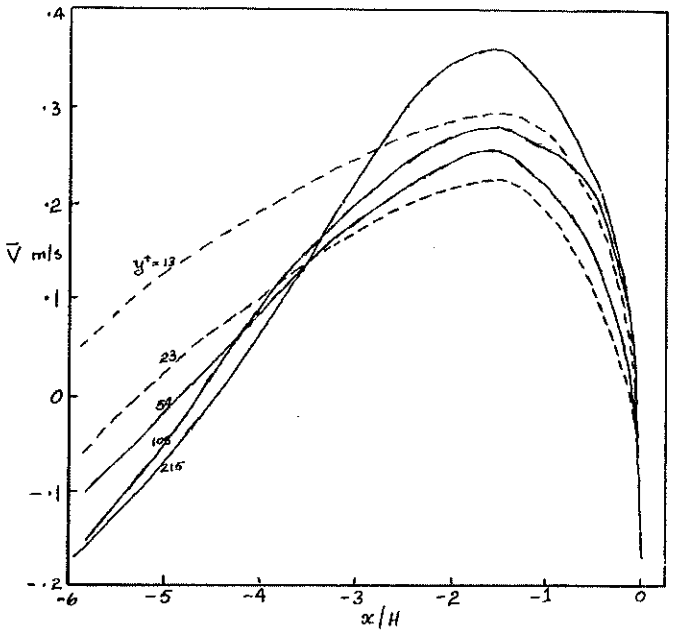

FIGURE 18. Distribution of $\overline{U}$ in the inner regions of the boundary layer, upstream from the step.

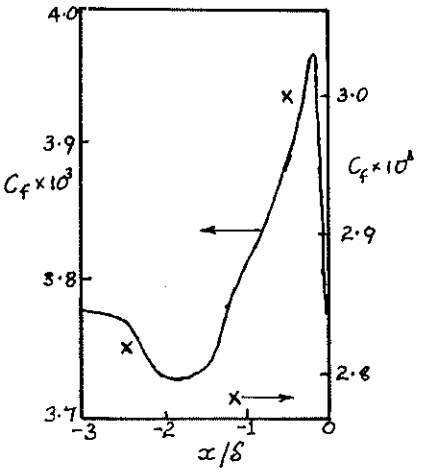

FIGURE 19. C_f values approaching the step.
— Our results, Figure 15. × Monsom et al (1981) results.

using modified TEACH programs, on flow over a backward facing step. In discussions with John Viegas concerning this work, John showed me the output from a program that he had run, using Sindir's algebraic stress model program. It was observed that the pressure values, and these values only, did indicate some influence upstream of the step - the negative pressures in the recirculating zone extending upstream about two step heights from the step. The extent of the negative zone, above the surface, was about half a step

height at the step, decreasing to zero at 2.5 step heights from the step. These pressure values, however, show non-monotonic changes, indicating that a finer grid is required in this region of the flow.

c) In his computational solution of the laminar flow over an aerofoil section, Jim Brown (EFD branch, NASA-Ames) showed that the C_f distribution had a distinct dip and then recovery just before reaching the trailing edge, in many ways emulating the curve of Figure 15.

We conclude that the upstream influence of the step is a feature of the flow and may be an important consideration when direct simulations of the flow are attempted.

9.6. Measurements Made Relating to the Large Scale Structures

To study the large scale structures in the flow, it was decided to carry out initial measurements in the boundary layer upstream of the step. There were two reasons for this choice. Firstly, there is available considerable published material on the large scale structures in a boundary layer. Our results could then be of a corroborative nature and also perhaps, by judicious placement of the sensors and analysis of the data, contribute to the understanding of these structures - particularly with regard to the influence, one on the other, of the outer and inner structures.

Secondly, any experimental and analysis techniques developed for this part of the flow could be applied equally well to the other regions of the flow — the "mixing layer" region and the region downstream of reattachment. All initial experiments were, therefore, carried out at $x = -100$mm ($x/H = -2.63$) where the step influence has hardly yet begun to have any major effect. For those measurements the floor plate was heated to a uniform temperature of about 10°C above the free-stream temperature, as described earlier.

The first experimental set-up consisted of two cold wire sensors at $y^+ \approx 10$ from the wall and separated from each other by $\Delta z^+ \approx 100$. The 3-wire miniature probe (X-wire + cold wire) was traversed between these two wires from $y^+ \approx 10$ to the outer regions of the boundary layer — data being taken at 30 stations. A typical time trace from the five sensors is shown in Figure 20.

Some structures can be discerned from the traces of the two wires closest to the wall. Sudden changes in the u signal also correspond to sudden changes in the temperature signals indicating that, as others have found, the u signal near the wall is a suitable structure detector.

The second experimental set-up, for investigating the large scale structures, consisted of 14 sensors. The previous 5 sensors were complemented by a further 5 cold wires arranged in a vertical array and 4 cold wires arranged in a horizontal array. Each of the wires in the vertical array was separated by approximately 5mm ($\Delta y^+ \approx 140$) while the wire that was closest to the wall was at $y^+ \approx 90$. To allow for the y traverse of the 3-wire sensor, it was necessary to offset the vertical array by about 4mm ($\Delta z^+ \approx 110$) from the centre-line of the traverse.

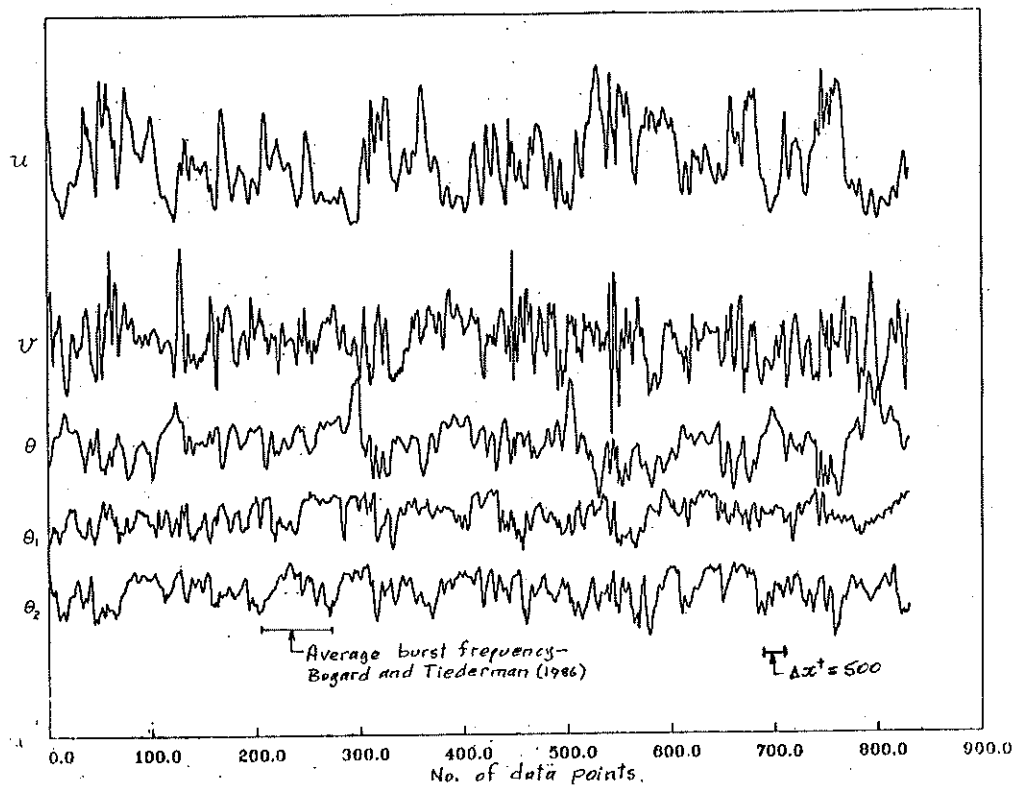

FIGURE 20. Time traces of velocity and temperature fluctuations. $x = -100$mm, $y^+ = 14$. θ: on 3-wire probe, θ_1 and θ_2: at $y^+ = 10$

The horizontal array had 2 wires on one side of the traverse centre-line and 2 wires on the other side. This array was situated at about the half-boundary-layer distance from the surface and spanned a total width of about 30mm ($\Delta z^+ \approx 840$). Data was obtained from all sensors as the 3-wire probe was moved to 30 stations across the boundary layer. Typical traces from the 14 sensors, obtained when the 3-wire probe was at $y = 14.8$mm ($y^+ = 415$) are shown in Figure 21.

A large scale structure can be noted as being detected simultaneously on a number of wires, as indicated by the crosses in Figure 21. The wire for θ_7 is obviously in the intermittent region of the flow.

A program was written to enable large scale structures to be detected, using data similar to Figure 20 or 21, by any single channel or combination of channels, using the WAG, Bisset et al (1958), method. This program was run and the detections made compared favorably with the "by-eye" detections using the time traces.

There was no time for further work by the author at this stage.

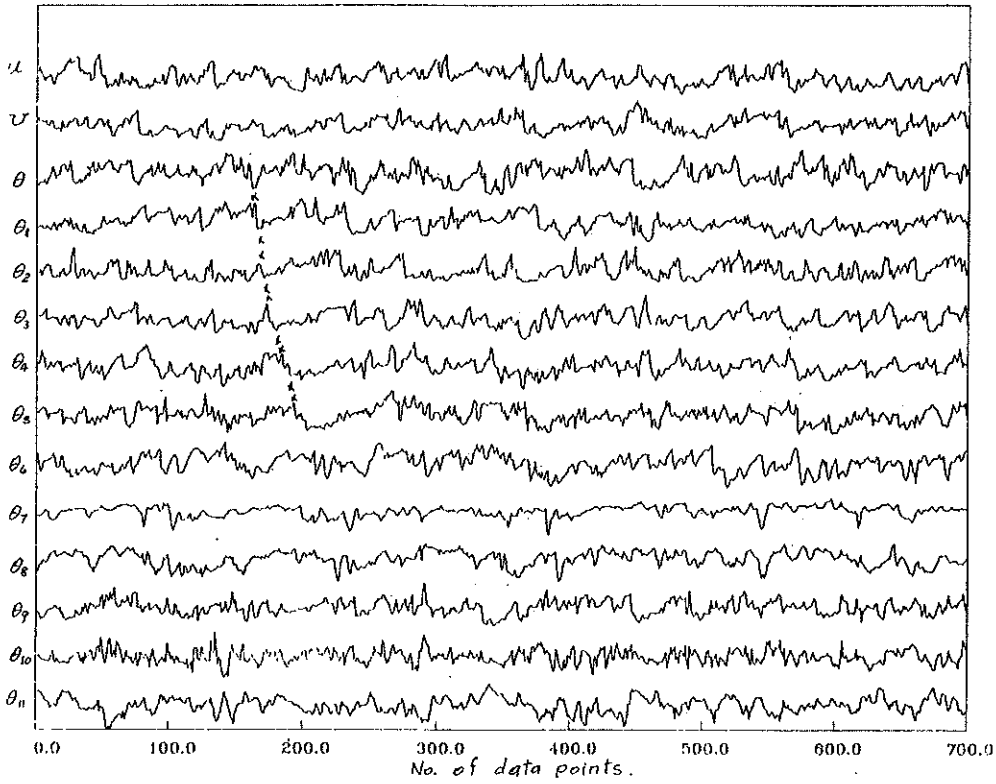

FIGURE 21. Typical time traces of velocity and temperature fluctuations using 3-wire probe (u, v, θ), 2 near-wall cold wires (θ_1, θ_2), a rake of 4 horizontal cold wires (θ_3 to θ_6), and a rake of 5 vertical cold wires (θ_7 to θ_{1_1}). $X = -100$mm, $y^+ = 415$.

10. Next Phase of the Work

Broadly, the next phase of the work is to apply the detections made using the above program to obtain conditionally sampled values of the velocities (u and v) at each station across the boundary layer. These values should be obtained for the inner and outer regions of the flow and also for, say, only those structures with the most common spacing. The results for structures with other spacings will also need to be checked. Some correlation work is necessary to determine the relative position of the conditioned velocities. Topologies of the inner and outer regions can then be built up and the distribution ("coherent" and "random") of momentum and heat transfer quantities determined. The other regions of the flow — the mixing layer and boundary layer after reattachment — can then be examined in a similar manner.

REFERENCES

ANDREOPOULOS, J., DURST, F., ZARIĆ, Z., & JOVANOVIĆ, J. 1984 Influence of Reynolds number on characteristics of turbulent wall boundary layers. *Exp't. in Fluids.* **2**, 7-16.

BISSET, D.K., ANTONIA, R.A., & BROWNE, L.W.B. 1988 Spatial organization of large structures in the turbulent far-wake of a cylinder. *J. Fluid Mech. (submitted)*

BOGARD, D. G., & TIERDERMAN, W. G. 1986 Burst detection with single-point velocity measurements. *J. Fluid Mech.* **162**, 389-413.

BRADSHAW, P. 1965 The effect of wind tunnel screens on nominally two-dimensional boundary layers. *J. Fluid Mech.* **22**, 679-687.

CLAUSER, F. H. 1954 Turbulent boundary layers in adverse pressure gradient. *J. Aero. Sci.* **21**

COLES, D. 1962 The turbulent boundary layer in a compressible fluid. Report No. R-403-PR, Rand Corp., Santa Monica.

DENGEL, P., & FERNHOLZ, H. H. 1988 Generation of and measurements in a turbulent boundary layer with zero skin friction. Second European Turbulence Conference, Technische Universitat Berlin, Poster Presentation, Topic F.

ECKELMANN, H. 1974 The structure of the viscous sublayer and the adjacent wall region in a turbulent channel flow. *J. Fluid Mech.* **65**, 439-459.

MEHTA, R. D., & HOFFMANN, P. H. 1987 Boundary layer two-dimensionality in wind tunnels. *Exp'ts. in Fluids.* **5**, 358-360.

MONSON, D. J., DRIVER, D. M., & SZODRUCH, J. 1981 Application of laser interferometer skin-friction meter in complex flows, IEEE publication, Proceedings of the International Congress on Instrumentation in Aerospace Simulation Facilities, Dayton, Ohio, pp. 232-243.

PATEL, V. C. 1965 Calibration of the Preston tube and limitation on its use in pressure gradients. *J. Fluid Mech.* **23**, 185-208.

PERRY, A. E., LIM, K. L., & HENBEST, S. M. 1987 An experimental study of the turbulence structure in smooth-and rough-wall boundary layers. *J. Fluid Mech.* **177**, 437-466.

SPALART, P. R. 1988 Direct simulation of a turbulent boundary layer up to $R_\theta = 1410$. *J. Fluid Mech.* **187**, 61-98.

SWEARINGEN, J. D., & BLACKWELDER, R. F. 1987 The growth and breakdown of streamwise vortices in the presence of a wall. *J. Fluid Mech.* **182**, 255-290.